Gauss's Principle With Inequality Constraints for Multiagent Navigation and Control

Boyang Zhang, *Student Member, IEEE*, and Henri P. Gavin

***Abstract*—Multiagent navigation systems present opportunities for many applications due to their agility and cooperation. In any multiagent navigation system, it is critical that actual interagent collisions are strictly prevented. In this article, we present a solution to the 2-D multiagent navigation problem with collision avoidance. Our solution to this problem is based on a novel extension to Gauss's principle of least constraint (GPLC), in which a fixed set of strict equality constraints is replaced by time-varying sets of active inequality constraints. To the best of our knowledge, this is the first instance that extends GPLC with dynamic incorporation and stabilization of active inequality constraints and with actuator delay and saturation. Herein, the dynamics of a collision-free multiagent system satisfies the Karush-Kuhn-Tucker conditions. Active inequality constraints enforce collision avoidance, leader following, and agglomeration behaviors, and they are stabilized using Baumgarte's error stabilization approach. We show that in dense configurations, the positional arrangement of the agents can lead to linearly dependent constraints, and we propose specialized solutions involving QR decomposition and regularization. The efficacy and efficiency of the proposed method are demonstrated by a dimensional analysis of a worst-case scenario and numerical studies of up to 100 agents tracking a prescribed virtual leader.**

***Index Terms*—Collision avoidance, constrained control, Gauss's principle of least constraint (GPLC), multiagent system navigation, optimal control.**

I. Introduction

IN AN age of automation, large-scale multiagent systems, such as swarms of unmanned aerial vehicles, autonomous vehicles, and autonomous underwater vehicles, are of increasing significance in diverse applications, such as exploration, surveillance, and disaster response [1], [2].

Currently, navigation and control of large-scale multiagent systems remains an open field [3]–[5]. As the dimension of the multiagent system increases, the computational cost for the controller becomes expensive for real-time implementation. Furthermore, collision avoidance, a critical requirement of multiagent system navigation, is inherently a nonconvex constraint, thus imposing additional challenge to the constrained optimization problem [6], [7].

According to [3], multiagent system navigation generally falls into two categories: planning and reacting. In the former approach, a global trajectory connecting the initial and goal configuration is planned for *each individual* agent and is updated as the plan is executed. In the latter method, however, no nominal path is planned *a priori*, and the agent heads toward the goal while reacting to its local environment (e.g., avoiding collisions, rejecting disturbances, etc.).

Optimization-based planning algorithms for multiagent system navigation typically involve iterative solutions to optimal control problems over a finite-time horizon or a physical length. These include quadratic programs (QP) (e.g., [8]–[13]), mixed-integer programs (e.g., [14]–[16]), and model predictive control methods (e.g., [17]–[21]). However, under some scenarios, these methods may not have a solution (e.g., [8] and [16]) or may have locally optimal solutions (e.g., [18] and [20]). Furthermore, the computational cost increases when the dimension of the multiagent system increases (e.g., [8], [14], and [15]). In addition, these approaches deal with the nonconvex optimization problem using sequential convex programming (SCP) (e.g., [13] and [20]) or integer programming (e.g., [14]–[17]). However, SCP may not converge to a globally optimal solution, and the integer program becomes intractable as the dimension becomes large.

Reactive methods include artificial potential methods and velocity obstacle based approaches. Artificial potential methods (e.g., [22]–[26]) impose potential functions over a configuration of agents in which the negative gradient of a superposition of artificial potential functions drives the agents toward the goals while repelling nearby pairs of agents from colliding with each other. However, the superposition of potential fields may lead to multiple local stationary point (e.g., [22]–[26]); thus, the agent may be trapped into local minima preventing navigation to the goal. Furthermore, the resulting control commands may exceed the actuator saturation bound (e.g., [22] and [23]), as the artificial potential and its gradient both go to infinity at the surface of an agent to prevent collisions.

Velocity obstacle methods define a set of all velocities that lead to the future collision of an agent-obstacle pair under the assumptions that all objects move at their current velocities and that any velocity can be instantaneously achieved (e.g., [27]–[29]). The velocity obstacle of an agent induced by all obstacles (other agents) are thus the union of convex cones corresponding

Manuscript received May 15, 2020; revised September 25, 2020; accepted January 30, 2021. Date of publication February 16, 2021; date of current version January 28, 2022. This work was supported in part by U.S. Army Research Office under Award 75 568-NS-II and in part by Duke University. Recommended by Associate Editor M. Cao. *(Corresponding author: Boyang Zhang.)*

The authors are with the Department of Civil and Environmental Engineering, Duke University, Durham, NC 27708 USA (e-mail: boyang.zhang@duke.edu; hpgavin@duke.edu).

Color versions of one or more figures in this article are available at https://doi.org/10.1109/TAC.2021.3059677.

Digital Object Identifier 10.1109/TAC.2021.3059677

to all agent-obstacle pairs. Hence, by choosing a velocity from the complement of this convex set in the velocity space, the agent will execute a collision-free trajectory. To overcome the unrealism imposed by the assumptions, acceleration-velocity obstacles [30] are proposed to refine the admissible velocity space by taking into account bounded accelerations. Though computationally cheap, velocity obstacle based approaches do not, in general, pursue globally optimal solution due to the nonconvex admissible velocity space [28]–[31].

The Udwadia-Kalaba (U-K) method [32] has been recently applied to the motion control of a unicycle-like mobile robot [33] and an artificial potential swarm [34]. The U-K equations represent the closed-form solution to Gauss's principle of least constraint (GPLC) [35]–[37] for the generalized forces of constraint and the constrained accelerations, in which Lagrange multipliers have been eliminated. By eliminating Lagrange multipliers, the U-K approach does not permit modeling actuator delay or actuator saturation. Furthermore, Lagrange multipliers are helpful diagnostic variables as they indicate the relative contribution of each constraint to the net control actions.

In a large-scale multiagent system, the exact assignment of the goal configuration and the planned trajectory for each individual agent may not be as important as that of the multiagent system as a whole [38]. Hence, each agent does not *actively* plan a path of any kind in the extension to GPLC presented here. Moreover, in most physical implementations, constraint violations are unavoidable, whether they arise from the natural evolution of the system, unmodeled actuator nonlinearity (e.g., saturation), unmodeled actuator dynamics (e.g., delay), or external disturbances. The performance of multiagent control schemes in which dynamics must adhere to hard constraints may be questioned if external disturbances and actuator nonlinearity/dynamics are significant and unmodeled. In addition, the requirement of multiagent system dynamics adhering to hard constraints may lead to control actions that exceed the achievable capacities of the actuator implemented. For these reasons, we propose a formulation that models actuator dynamics and saturation, that is able to stabilize violated constraints to feasible configurations, and that can easily incorporate exogenous disturbances in the formulation.

A. Contributions and Outline

In this article, we propose a framework for guiding multiagent systems in a compact and noncolliding configuration while following the trajectory of a prescribed virtual leader. The framework extends GPLC by 1) dynamically incorporating active inequality constraints, 2) dynamically enforcing a second-order asymptotic convergence to the admissible space for all active constraints, and 3) saturating and delaying the GPLC generalized constraint forces to compute true constrained agent accelerations.

The first contributions of this article are these extensions of GPLC in the control of any system. To the best of our knowledge, the present article is the first to apply GPLC to feedback control with actuator delay and saturation and is the first to show how the time-varying set of active inequality constraints are identified.

By differentiating the nonconvex collision avoidance constraints so that the resulting differentiated constraints become linear in acceleration and by incorporating these linear constraints into a Karush-Kuhn-Tucker (KKT) system, we convert a nonconvex problem into its convex counterpart and obtain a globally optimal solution. This is the second contribution of our article, which contrasts with the use of first-order approximations of the nonconvex constraints in an iterative SCP solution (e.g., [9] and [13]) or an approximation by a convex subset of the admissible space (e.g., [8] and [30]).

The third contribution of this approach is the essential ability of the system to recover from inadmissible initial conditions and constraint violations. In contrast to many methods' conservatism that requires all agents to start from admissible states and to adhere to hard constraints at all times (e.g., [10]–[12]), the extended GPLC framework allows multiagent systems to start from inadmissible initial states and endows the systems with the resiliency to smoothly recover from inadmissible positions. Indeed, the approach presented here intentionally allows for constraint violations as control actions arise only from slightly violated inequality constraints. In order to limit constraint violations within acceptable limits and without exceeding actuation capacity bounds, GPLC control parameters may be selected according to a dimensional analysis presented here. In Section VI-B, we show how these parameters can be chosen to guarantee collision avoidance with the least effort for given system characteristics under a proposed worst-case scenario. This is in contrast to the highly parameterized and comparatively abstract approaches previously considered (e.g., [23]).

Fourth, this article pertains to solving for a unique admissible solution when the multiagent system is subject to linearly dependent constraints. Our approach enables the algorithm to 1) identify configurations in which the equations of state are not unique and to 2) automatically adapt itself to provide sensible control actions at every time step. We present specialized methods based on QR decomposition and regularization to identify and resolve rank-deficiency issues, which are more efficient than using the Moore-Penrose generalized inverse (e.g., [34]).

A fifth feature of our approach is its mathematical simplicity and computational efficiency. In contrast to some prior optimization-based planning approaches that minimize an integral over a finite-time horizon (e.g., [8]), which is computationally unaffordable for real-time implementation for a large number of agents (e.g., [15]), our control system requires only the formulation and solution of a matrix equation at each time step without iteration. These computations are amenable to real-time implementations on high-dimensional systems.

The article is organized as follows. In Section II, we review GPLC, the existence and uniqueness of the solution to a KKT system, and Baumgarte's error stabilization scheme. Then, Section III formulates the multiagent navigation and control (MANC). Next, Section IV addresses the possible issues of solving the MANC problem, followed by two remedies introduced in Section V. Numerical results and discussions are presented in Section VI. Finally, the conclusions and future work can be found in Section VII.

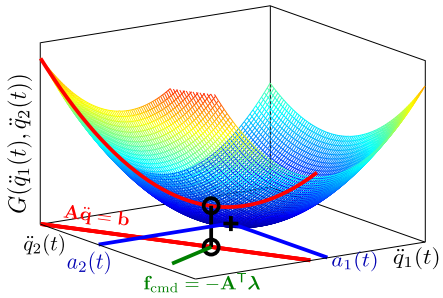

Fig. 1. Equation of motion in constrained systems with a symmetric positive-definite mass matrix is the unique minimum of the projection of $\mathbf{A}\ddot{\mathbf{q}} = \mathbf{b}$ onto $G \triangleq (\ddot{\mathbf{q}} - \mathbf{a})^\mathsf{T}\mathbf{M}(\ddot{\mathbf{q}} - \mathbf{a})$, where the unconstrained equations of motion are $\mathbf{M}\mathbf{a} = \mathbf{f}$.

II. Preliminaries

This article extends GPLC to dynamically enforce holonomic inequality constraints. The resulting equations of motion enforce constraints through forces related to the Lagrange multipliers.

A. Gauss's Principle of Least Constraint

In 1829, Gauss [35] formulated a flexible method for adjoining constraints to dynamical systems. In this section, we provide a novel interpretation of GPLC. In a dynamical system with position coordinates defined by the vector $\mathbf{q}(t)$, the unconstrained accelerations $\mathbf{a}$ are related to the net forces due to internal and external actions through Newton's second law

$$\mathbf{M}\,\mathbf{a} = \mathbf{f}\,. \tag{1}$$

In this article, $\mathbf{M} \in \mathbb{R}^{2N\times 2N}$ is a symmetric positive-definite (SPD) mass matrix, where N is the number of agents of a multiagent system, the coordinate position vector $\mathbf{q} \in \mathbb{R}^{2N}$, and $\mathbf{f}$ is a vector that contains all other noninertial forces, potentially including exogenous disturbances. (The effect of exogenous disturbances on the control performance of our approach is left to a future study.) Note here that for an SPD $\mathbf{M}$, Newton's second law (1) solves

$$\min_{\ddot{\mathbf{q}}} \frac{1}{2}\ddot{\mathbf{q}}^\mathsf{T}\mathbf{M}\ddot{\mathbf{q}} - \mathbf{f}^\mathsf{T}\ddot{\mathbf{q}}\,. \tag{2}$$

Actions of constraints may be imposed on this minimization in order to enforce geometric relationships amongst the coordinate positions and velocities

$$\mathbf{g}(\mathbf{q}, \dot{\mathbf{q}}, t) = \mathbf{0}\,. \tag{3}$$

In the control of the multiagent systems considered in this analysis, all the constraints are relations among the coordinate positions. Thus, the discussion herein pertains only to the holonomic constraints, even though GPLC is also capable of deriving the equations of motion for nonholonomically constrained systems.

Applying GPLC to holonomically constrained systems requires that the constraints are at least twice differentiable in time. To incorporate inequality constraints $\mathbf{h}(\mathbf{q}, t) \leqslant \mathbf{0}$ in a dynamic context of GPLC, we identify the set of active constraints as the positive-valued subset of $\mathbf{h}$ and enforce them as equality constraints. Doing so solves the primary challenge of (static) QP problems, i.e., identifying the set of active constraints [6]. If other equality constraints are at hand, they would be included in the set of active constraints, and they must be at least differentiable to the orders such that the differentiated constraints are linear in accelerations $\ddot{\mathbf{q}}$.

We proceed with a set of C active constraints on coordinate positions

$$\mathbf{g}(\mathbf{q}, t) = \mathbf{0} \tag{4}$$

where $\mathbf{g} : \mathbb{R}^{2N+1} \to \mathbb{R}^C$. Differentiating $\mathbf{g}$ twice with respect to time, these constraints become linear in the coordinate accelerations

$$\frac{d^2}{dt^2}\mathbf{g}(\mathbf{q}, t) = \frac{\partial \mathbf{g}}{\partial \mathbf{q}}\ddot{\mathbf{q}} + \frac{d}{dt}\left(\frac{\partial \mathbf{g}}{\partial \mathbf{q}}\right)\dot{\mathbf{q}} + \frac{d}{dt}\left(\frac{\partial \mathbf{g}}{\partial t}\right) = \mathbf{0} \tag{5}$$

which may be compactly written as

$$\mathbf{A}(\mathbf{q}, t)\,\ddot{\mathbf{q}} = \mathbf{b}(\mathbf{q}, \dot{\mathbf{q}}, t) \tag{6}$$

where

$$\mathbf{A}(\mathbf{q}, t) = \frac{\partial \mathbf{g}}{\partial \mathbf{q}} = \begin{bmatrix} \frac{\partial g_1(\mathbf{q},t)}{\partial q_1} & \cdots & \frac{\partial g_1(\mathbf{q},t)}{\partial q_{2N}} \\ \vdots & \ddots & \vdots \\ \frac{\partial g_C(\mathbf{q},t)}{\partial q_1} & \cdots & \frac{\partial g_C(\mathbf{q},t)}{\partial q_{2N}} \end{bmatrix}$$

is the Jacobian matrix of $\mathbf{g}$ with respect to $\mathbf{q}$.

Note that enforcing (6) does not necessarily satisfy (4). In Section II-C, we address this issue with Baumgarte's asymptotic constraint error stabilization scheme [39] that drives $\mathbf{g}(\mathbf{q}, t)$ to zero.

With double-differentiated active constraints on the coordinate positions, the constrained equations of motion may be expressed through a constrained minimization principle

$$\min_{\ddot{\mathbf{q}}} \frac{1}{2}\ddot{\mathbf{q}}^\mathsf{T}\mathbf{M}\ddot{\mathbf{q}} - \mathbf{f}^\mathsf{T}\ddot{\mathbf{q}} \quad \text{s.t.} \quad \mathbf{A}\ddot{\mathbf{q}} = \mathbf{b} \tag{7}$$

which is equivalent to

$$\max_{\boldsymbol{\lambda}} \min_{\ddot{\mathbf{q}}} \frac{1}{2}\ddot{\mathbf{q}}^\mathsf{T}\mathbf{M}\ddot{\mathbf{q}} - \mathbf{f}^\mathsf{T}\ddot{\mathbf{q}} + \boldsymbol{\lambda}^\mathsf{T}(\mathbf{A}\ddot{\mathbf{q}} - \mathbf{b}) \tag{8}$$

where $\boldsymbol{\lambda} \neq \mathbf{0}$ are Lagrange multipliers that enforce the differentiated active inequality constraints.

To arrive upon Gauss's definition of the principle of least constraint, we add $\frac{1}{2}\mathbf{a}^\mathsf{T}\mathbf{M}\mathbf{a}$ to the augmented objective (8) without changing its solution

$$\max_{\boldsymbol{\lambda}} \min_{\ddot{\mathbf{q}}} \frac{1}{2}\ddot{\mathbf{q}}^\mathsf{T}\mathbf{M}\ddot{\mathbf{q}} - \ddot{\mathbf{q}}^\mathsf{T}\mathbf{f} + \frac{1}{2}\mathbf{a}^\mathsf{T}\mathbf{M}\mathbf{a} + \boldsymbol{\lambda}^\mathsf{T}(\mathbf{A}\ddot{\mathbf{q}} - \mathbf{b})\,. \tag{9}$$

After substituting (1) into (9), we can equate the objective (8) to

$$\max_{\boldsymbol{\lambda}} \min_{\ddot{\mathbf{q}}} \frac{1}{2}(\ddot{\mathbf{q}} - \mathbf{a})^\mathsf{T}\mathbf{M}(\ddot{\mathbf{q}} - \mathbf{a}) + \boldsymbol{\lambda}^\mathsf{T}(\mathbf{A}\ddot{\mathbf{q}} - \mathbf{b})\,. \tag{10}$$

This is the constrained minimization conceived by Gauss, which states that in a constrained system, the true accelerations minimize the mass-weighted quadratic form of the difference between the true constrained accelerations and the unconstrained accelerations, subject to double-differentiated constraints. The

solution to these linearly constrained quadratic minimizations satisfies KKT conditions

$$\begin{bmatrix} \mathbf{M} & \mathbf{A}^\intercal \\ \mathbf{A} & \mathbf{0} \end{bmatrix} \begin{bmatrix} \ddot{\mathbf{q}} \\ \boldsymbol{\lambda} \end{bmatrix} = \begin{bmatrix} \mathbf{f} \\ \mathbf{b} \end{bmatrix} \tag{11}$$

which represent the saddle point of the augmented objective. The KKT system (11) is a system of $2N + C$ equations that are linear in $2N + C$ unknowns, $[\ddot{\mathbf{q}}^\intercal \quad \boldsymbol{\lambda}^\intercal]^\intercal$. In the constrained equations of motion, $-\mathbf{A}^\intercal\boldsymbol{\lambda}$ are the actions that enforce the constraints [36]. Note that the resulting control scheme is nonlinear and discontinuous for the multiagent system studied in this article.

B. Existence and Uniqueness of the Solution to KKT Systems

Proposition 1: For multiagent systems considered in this study, the KKT system (11) is singular if and only if $\mathbf{A}^\intercal$ has a nontrivial null space.

Proof: First, we note that $\mathbf{M} \in \mathbb{R}^{2N\times 2N}$ is a diagonal and SPD matrix for an N-agent system considered in this study; so it has no nontrivial null space $\ddot{\mathbf{q}}$ to intersect the null space of $\mathbf{A}$.

1) $\Rightarrow$: If $\exists[\ddot{\mathbf{q}}^\intercal \quad \boldsymbol{\lambda}^\intercal]^\intercal \neq \mathbf{0}$ that lies within the nontrivial null space of the KKT matrix, then $\mathbf{A}\ddot{\mathbf{q}} = \mathbf{0}$, implying that either $\ddot{\mathbf{q}} = \mathbf{0}$ or $\ddot{\mathbf{q}} \in \mathcal{N}(\mathbf{A})$. If $\ddot{\mathbf{q}} = \mathbf{0}$, then $\mathbf{A}^\intercal\boldsymbol{\lambda} = \mathbf{0}$, indicating that either $\boldsymbol{\lambda} = \mathbf{0}$ or $\boldsymbol{\lambda} \in \mathcal{N}(\mathbf{A}^\intercal)$. But $[\ddot{\mathbf{q}}^\intercal \quad \boldsymbol{\lambda}^\intercal]^\intercal = \mathbf{0}$ is trivial. So if the KKT system is singular and $\ddot{\mathbf{q}} = \mathbf{0}$, then $\exists\, \boldsymbol{\lambda} \neq \mathbf{0}$ such that $\boldsymbol{\lambda} \in \mathcal{N}(\mathbf{A}^\intercal)$.
2) $\Leftarrow$: If $\exists\, \boldsymbol{\lambda} \neq \mathbf{0}$ such that $\mathbf{A}^\intercal\boldsymbol{\lambda} = \mathbf{0}$, then $\ddot{\mathbf{q}} = \mathbf{0}$ solves $\mathbf{M}\ddot{\mathbf{q}} + \mathbf{A}^\intercal\boldsymbol{\lambda} = \mathbf{0}$. Thus, $[\mathbf{0}^\intercal \quad \boldsymbol{\lambda}^\intercal]^\intercal$ is a nontrivial null space of the KKT matrix; therefore, the KKT system is singular. If the system of constraints are linearly dependent, then any Lagrange multiplier in $\mathcal{N}(\mathbf{A}^\intercal)$ associates with constraint forces of zero.

C. Stabilization of Active Constraints

In the presence of inadmissible initial states, exogenous forcing, and actuation or sensing delays, the trajectories may not adhere to one or more constraint. In this application of GPLC to the control of multiagent systems, we allow constraints to be violated and asymptotically stabilize the dynamics of the constraints to zero. This approach, called Baumgarte's stabilization [39], introduces additional constraint dynamics by replacing $\ddot{g} = 0$ with

$$\ddot{g} + 2\zeta\omega\dot{g} + \omega^2 g = 0 \tag{12}$$

where $g \in \mathbf{g}(\mathbf{q}, t)$ is any active constraint that is linearly independent of all the other active constraints in $\mathbf{g}(\mathbf{q}, t)$.

Applications of Baumgarte's stabilization method require the problem-dependent tuning of the Baumgarte constants ζ and ω so that constraint violations quickly stabilize to acceptably small values. Ostermeyer [40] suggests $\zeta = \sqrt{2}/2$ and ω less than the highest resonant frequency of the unconstrained system. As the ζ and ω values required for these purposes can lead to instability in the numerical integration method [41], the second-order system of Baumgarte's approach can be replaced by a sliding-mode oscillator [42] that converges linearly to $g = 0$. For fixed-step fourth-order Runge-Kutta integration, Lin and Huang [43] suggest values of $\omega \approx \pi/(\Delta t)$ and $\zeta \approx 1/2$ to preserve numerical stability. Alternatively, Sparschuh and Hagedorn [44] present a constraint error elimination method tailored to the numerical integration scheme. Other such methods are reviewed by Bauchau and Laulusa [41]. Extending Baumgarte's method to higher order differential algebraic equations (DAEs) complicates the selection of the stabilization constants as the constraint equations must be differentiated to the highest order in the system of DAEs, resulting in a larger number of constants [45].

In Section VI-B, we provide a systematic approach for specifying values of the Baumgarte constants to guarantee collision avoidance for a specified worst-case scenario, wherein the stabilization goals are to smoothly adjust agent trajectories within an allowable period of time and within available actuation authority in order to avoid a collision. Importantly, in contrast to the Baumgarte's stabilization of kinematic constraints, stabilization of constraints in multiagent control can permit larger and longer constraint violation, with correspondingly smaller constraint (control) forces.

Equation (12) can be expanded as

$$\frac{\partial g}{\partial \mathbf{q}}\ddot{\mathbf{q}} + \frac{d}{dt}\left(\frac{\partial g}{\partial \mathbf{q}}\right)\dot{\mathbf{q}} + \frac{d}{dt}\left(\frac{\partial g}{\partial t}\right) + 2\zeta\omega\left(\frac{\partial g}{\partial \mathbf{q}}\dot{\mathbf{q}} + \frac{\partial g}{\partial t}\right) + \omega^2 g = 0\,. \tag{13}$$

Applying (13) to all active constraints $\mathbf{g}$ at each time step and representing them in a more compact manner, we have

$$\mathbf{A}(\mathbf{q}, t)\,\ddot{\mathbf{q}} = \hat{\mathbf{b}}(\mathbf{q}, \dot{\mathbf{q}}, t) \tag{14}$$

where $\hat{\mathbf{b}}$ now contains terms involving ω and ζ. Compared to $\mathbf{b}$ in (6), ω and ζ may be respectively interpreted as the natural frequency and damping ratio of the *constraint oscillator* $g(t)$ and, therefore, may be regarded as control parameters.

Hence, the GPLC objective (10) incorporated with the stabilization of active constraints can be expressed as

$$\max_{\boldsymbol{\lambda}} \min_{\ddot{\mathbf{q}}} \frac{1}{2}(\ddot{\mathbf{q}} - \mathbf{a})^\intercal\mathbf{M}(\ddot{\mathbf{q}} - \mathbf{a}) + \boldsymbol{\lambda}^\intercal(\mathbf{A}\ddot{\mathbf{q}} - \hat{\mathbf{b}}) \tag{15}$$

whose solution satisfying KKT system (11) integrated with constraint error stabilization can be expressed as

$$\begin{bmatrix} \mathbf{M} & \mathbf{A}^\intercal \\ \mathbf{A} & \mathbf{0} \end{bmatrix} \begin{bmatrix} \ddot{\mathbf{q}} \\ \boldsymbol{\lambda} \end{bmatrix} = \begin{bmatrix} \mathbf{f} \\ \hat{\mathbf{b}} \end{bmatrix}\,. \tag{16}$$

The equivalence of (15) and (16) implies that constrained dynamical systems modeled by (16) may be interpreted through the perspective of GPLC (15) with Baumgarte's stabilization driving constraint violations asymptotically to zero. The formulation of (16) is well known in the field of constrained multibody dynamics [40]–[45] in which kinematic constraints (such as contact and inextensibility) must be satisfied within tight tolerances.

III. Mathematical Formulation of Multiagent Swarm Navigation

Restricting our presentation to motions in a 2-D plane, we note that this approach is amenable to 3-D motions. We consider N agents moving in a 2-D plane, with constant masses m_i and position coordinates (x_i, y_i) for agents $i \in \{1, 2, \ldots, N\}$.

A. Unconstrained Dynamics

In 2-D, an unconstrained agent at coordinates (x_i, y_i) in a multiagent system is free to move without consideration of potential collisions, leader following, or swarm compactness. The unconstrained agent is forced only by exogenous process, and its equations of motion are expressed as

$$\begin{bmatrix} m_i & 0 \\ 0 & m_i \end{bmatrix} \begin{bmatrix} \ddot{x}_i \\ \ddot{y}_i \end{bmatrix} = \begin{bmatrix} f_{ix} \\ f_{iy} \end{bmatrix} \tag{17}$$

where f_X and f_Y are the external forces on agent i along X and Y directions, which could result from environmental or adversarial actions.

B. Constraints

Constraining all agents to be within a radius R from a virtual leader at $(\bar{x}(t), \bar{y}(t))$, we define the leader following constraint for agent i by

$$g_{\mathrm{f}_i} \triangleq (x_i - \bar{x})^2 + (y_i - \bar{y})^2 - R^2 \leqslant 0\,. \tag{18}$$

Note that the constraints g_{f_i}, $\forall i \in \{1, 2, \ldots, N\}$, enforce both leader following and swarm compactness goals, where the swarm compactness is defined in terms of the deviation between the swarm centroid and the virtual leader, i.e.,

$$D_{\mathrm{c}} \triangleq \sqrt{\left(\frac{1}{N}\sum_{i=1}^{N} x_i - \bar{x}\right)^2 + \left(\frac{1}{N}\sum_{i=1}^{N} y_i - \bar{y}\right)^2}\,. \tag{19}$$

Moreover, interagent collisions must be avoided during the evolution of the swarm. Hence, we define the collision avoidance constraint for agent pair $\{i, j\}$, $\forall i < j$, $i, j \in \{1, 2, \ldots, N\}$, as

$$g_{\mathrm{c}_{ij}} \triangleq d_{ij}^2 - (x_i - x_j)^2 - (y_i - y_j)^2 \leqslant 0 \tag{20}$$

where $d_{ij} = d_{ji}$ is the minimum safety distance between agent i and agent j. We define a safety buffer around agent i as a circle of radius r_i such that $r_i + r_j = d_{ij}$. The most challenging case for collision avoidance is if two agents move directly toward each other at a maximum attainable speed $V_{\max}$. Hence, if the buffer size is greater than the peak response of this most extreme scenario, then no collision avoidance constraint violations can lead to actual interagent collisions.

Note that (20) are nonconvex constraints, but they can be dealt with in our framework without impairing the globally uniqueness of the solution.

C. Constraint Error Stabilization

Assuming that n_{f} agents and n_{c} pairs of agents violate (18) and (20) at a time instant, respectively, then $0 \leqslant n_{\mathrm{f}} \leqslant N$ and $0 \leqslant n_{\mathrm{c}} \leqslant \frac{N(N-1)}{2}$. We denote $\mathbb{S}_{\mathrm{f}}$ and $\mathbb{S}_{\mathrm{c}}$ as the active sets that contain the indices for each deviating agent i and each colliding pair $\{i, j\}$, respectively. Note that only $\{i, j\}$, rather than both $\{i, j\}$ and $\{j, i\}$, is kept track of in $\mathbb{S}_{\mathrm{c}}$ to eliminate repeating (and thus linear dependency between) constraints.

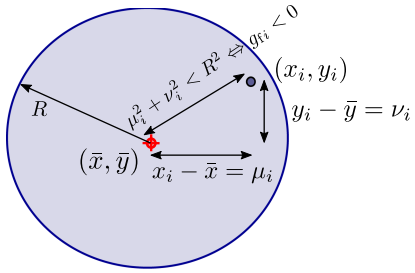

Fig. 2. Illustration of variables for leader following constraint.

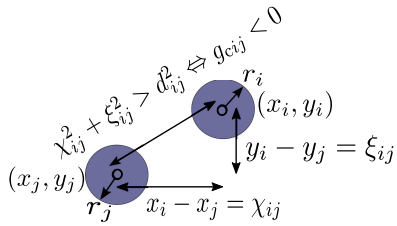

Fig. 3. Illustration of variables for collision avoidance constraint.

Note also that x_i, x_j, y_i, y_j, $\bar{x}$, and $\bar{y}$ in (18) and (20) are all functions of time t. Taking the first- and second-order time derivative of g_{f_i} and $g_{\mathrm{c}_{ij}}$, respectively, we obtain

$$\begin{aligned} \dot{g}_{\mathrm{f}_i} &= 2(\mu_i\dot{\mu}_i + \nu_i\dot{\nu}_i) \\ \ddot{g}_{\mathrm{f}_i} &= 2(\dot{\mu}_i^2 + \dot{\nu}_i^2 + \mu_i\ddot{\mu}_i + \nu_i\ddot{\nu}_i) \end{aligned} \tag{21}$$

$$\begin{aligned} \dot{g}_{\mathrm{c}_{ij}} &= 2(\chi_{ji}\dot{\chi}_{ij} + \xi_{ji}\dot{\xi}_{ij}) \\ \ddot{g}_{\mathrm{c}_{ij}} &= 2(\chi_{ji}\ddot{\chi}_{ij} + \xi_{ji}\ddot{\xi}_{ij} - \dot{\chi}_{ji}^2 - \dot{\xi}_{ji}^2) \end{aligned} \tag{22}$$

where $\mu_i = x_i - \bar{x}$, $\nu_i = y_i - \bar{y}$, $\chi_{ij} = x_i - x_j$, $\xi_{ij} = y_i - y_j$, and the overdots denote the differentiation with respect to time.

Figs. 2 and 3 illustrate the variables for leader following and collision avoidance constraint, respectively. Note that agents are respectively represented by their centroids in Figs. 2 and 3. We can always analyze the multiagent swarm given the actual size of an agent l by replacing the condensed centroids with circles that enclose the actual volume of an agent. Thus, l is omitted from the formulation in this section.

In this formulation, all the active constraints are stabilized by the second-order Baumgarte's error stabilization approach [39], which states that

$$\begin{aligned} \ddot{g}_{\mathrm{f}_i} + 2\zeta_{\mathrm{f}}\omega_{\mathrm{f}}\dot{g}_{\mathrm{f}_i} + \omega_{\mathrm{f}}^2 g_{\mathrm{f}_i} = 0, \quad \forall i \in \mathbb{S}_{\mathrm{f}} \\ \ddot{g}_{\mathrm{c}_{ij}} + 2\zeta_c\omega_{\mathrm{c}}\dot{g}_{\mathrm{c}_{ij}} + \omega_{\mathrm{c}}^2 g_{\mathrm{c}_{ij}} = 0, \quad \forall \{i, j\} \in \mathbb{S}_{\mathrm{c}} \end{aligned} \tag{23}$$

where ζ_{f}, ω_{f}, ζ_{c}, and ω_{c} are the damping ratio and natural frequency for active leader following and collision avoidance constraint, respectively. Note that for a heterogeneous multiagent system, each constraint may be stabilized with different values of ζ_{f}, ω_{f}, ζ_{c}, and ω_{c}.

D. Karush-Kuhn-Tucker System

By incorporating the unconstrained dynamics (17) with the stabilized differentiated constraints (23), the constrained dynamics of the multiagent system satisfies the KKT system (16)

$$\begin{bmatrix} \mathbf{M} & \mathbf{A}_{g_\mathrm{f}}^\intercal & \mathbf{A}_{g_\mathrm{c}}^\intercal \\ \mathbf{A}_{g_\mathrm{f}} & \mathbf{0} & \mathbf{0} \\ \mathbf{A}_{g_\mathrm{c}} & \mathbf{0} & \mathbf{0} \end{bmatrix} \begin{bmatrix} \ddot{\mathbf{q}} \\ \boldsymbol{\lambda}_{g_\mathrm{f}} \\ \boldsymbol{\lambda}_{g_\mathrm{c}} \end{bmatrix} = \begin{bmatrix} \mathbf{f} \\ \hat{\mathbf{b}}_{g_\mathrm{f}} \\ \hat{\mathbf{b}}_{g_\mathrm{c}} \end{bmatrix} \tag{24}$$

where $\mathbf{f}$ may contain any exogenous force, and the rows of $\mathbf{A}_{g_\mathrm{f}}$ and $\mathbf{A}_{g_\mathrm{c}}$ and the corresponding right-hand sides are respectively

$$\begin{aligned} \mathbf{a}_{g_{\mathrm{f}_i}} &= 2\begin{bmatrix} \mathbf{0} & \mu_i & \nu_i & \mathbf{0} \end{bmatrix} \\ \mathbf{a}_{g_{\mathrm{c}_{ij}}} &= 2\begin{bmatrix} \mathbf{0} & \chi_{ji} & \xi_{ji} & \mathbf{0} & \chi_{ij} & \xi_{ij} & \mathbf{0} \end{bmatrix} \\ \hat{b}_{g_{\mathrm{f}_i}} &= -2\left(\dot{\mu}_i^2 + \dot{\mu}_i^2 - \mu_i \dddot{\bar{x}} - \nu_i \dddot{\bar{y}}\right) - 2\zeta_\mathrm{f}\omega_\mathrm{f}\dot{g}_{\mathrm{f}_i} - \omega_\mathrm{f}^2 g_{\mathrm{f}_i} \\ \hat{b}_{g_{\mathrm{c}_{ij}}} &= 2\dot{\chi}_{ij}^2 + 2\dot{\xi}_{ij}^2 - 2\zeta_c\omega_\mathrm{c}\dot{g}_{\mathrm{c}_{ij}} - \omega_\mathrm{c}^2 g_{\mathrm{c}_{ij}} \,. \end{aligned} \tag{25}$$

Denoting the number of active g_f and g_c at each time instant as n_f and n_c, respectively, then $\mathbf{A}_{g_\mathrm{f}} \in \mathbb{R}^{n_\mathrm{f}\times 2N}$, $\mathbf{A}_{g_\mathrm{c}} \in \mathbb{R}^{n_\mathrm{c}\times 2N}$. If agent i is the p-th element in $\mathbb{S}_\mathrm{f}$, then $\mathbf{a}_{g_{\mathrm{f}_i}}$ is the p-th row of $\mathbf{A}_{g_\mathrm{f}}$ with the entries μ_i and ν_i on the $(2i-1)$-th and $(2i)$-th column, respectively. Similarly, if agent pair $\{i,j\}$ is the q-th element in $\mathbb{S}_\mathrm{c}$, then $\mathbf{a}_{g_{\mathrm{c}_{ij}}}$ is the q-th row of $\mathbf{A}_{g_\mathrm{c}}$ with the entries χ_{ji}, ξ_{ji}, χ_{ij}, and ξ_{ij} on the $(2i-1)$-th, $(2i)$-th, $(2j-1)$-th, and $(2j)$-th column, respectively. $\hat{b}_{g_{\mathrm{f}_i}}$ and $\hat{b}_{g_{\mathrm{c}_{ij}}}$ are the right-hand side scalars in $\hat{\mathbf{b}}_{g_{\mathrm{f}_i}}$ and $\hat{\mathbf{b}}_{g_{\mathrm{c}_{ij}}}$ that correspond to $\mathbf{a}_{g_{\mathrm{f}_i}}$ and $\mathbf{a}_{g_{\mathrm{c}_{ij}}}$, respectively. Note that the numbers of rows of $\mathbf{A}_{g_\mathrm{f}}$ and $\mathbf{A}_{g_\mathrm{c}}$ change over time depending on the natural evolution of the constrained system dynamics.

E. Selection of Control Parameters

The response of the autonomous second-order constraint dynamics is

$$\begin{bmatrix} g(t) \\ \dot{g}(t) \end{bmatrix} = e^{\Phi t} \begin{bmatrix} g(t_0) \\ \dot{g}(t_0) \end{bmatrix} \tag{26}$$

where t_0 denotes the time instant at which the dynamics of $g(t)$ is initiated, and the matrix exponential $e^{\Phi t}$ is given in (27) [46], where $\omega_\mathrm{d} = \omega\sqrt{|1-\zeta^2|}$ is the damped natural frequency of the constraint dynamics.

Therefore, the second-order constraint dynamics (12) can be analytically determined given the initial conditions for the constraint. Note that (26) is enforced only when the corresponding constraint becomes active, thus resulting in discontinuous control laws. Introducing the assumption that all given trajectories and agents have zero initial velocities, i.e., $\dot{g}(0) = 0$, a constraint g may be violated either at $t = 0$, i.e., due to inadmissible initial positions, or at some $t > 0$ when it changes from nonpositive to positive values during the evolution of the system dynamics. Thus, we have two possible types of initial conditions for the second-order dynamics of any active constraint $g(t)$:

1) **Case 1:** $g(t_0) > 0$ and $\dot{g}(t_0) = 0$, when $t_0 = 0$;
2) **Case 2:** $g(t_0) = 0$ and $\dot{g}(t_0) > 0$, when $t_0 > 0$.

To obtain the maximum constraint violation g_max for given initial conditions, we solve for the first time instant t such that $\dot{g}(t) = 0$, and we denote this t as t_max. Then, we can obtain g_max by evaluating $g(t)$ at $t = t_\mathrm{max}$. Note that for the two types of initial conditions, either $g(t_0)$ or $\dot{g}(t_0)$ is zero.

After some algebraic manipulations, we obtain

$$\begin{aligned} g_\mathrm{max} &= g(0), && \text{for Case 1} \\ g_\mathrm{max} &= \frac{\dot{g}(t_0)}{\omega} e^{-\zeta\omega t_\mathrm{max}} = \frac{\dot{g}(t_0)}{\omega} e^{\eta(\zeta)}, && \text{for Case 2} \end{aligned} \tag{28}$$

where

$$e^{\eta(\zeta)} = \begin{cases} e^{\frac{-\zeta}{\sqrt{1-\zeta^2}} \arctan \frac{\sqrt{1-\zeta^2}}{\zeta}}, & 0 < \zeta < 1 \\ e^{-\zeta}, & \zeta = 1 \\ e^{\frac{-\zeta}{\sqrt{\zeta^2-1}} \ln\left(\zeta + \sqrt{\zeta^2-1}\right)}, & \zeta > 1 \end{cases} \tag{29}$$

is a single-variable function in ζ and decreases exponentially as ζ increases.

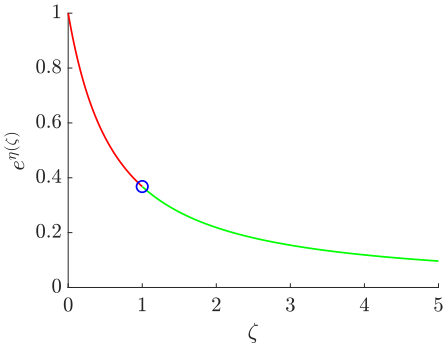

Fig. 4. Plot of $e^{\eta(\zeta)}$ for Case 2 initial conditions as a function of ζ, where $0 < \zeta \leqslant 5$.

$$e^{\Phi t} = \begin{cases} e^{-\zeta\omega t}\begin{bmatrix} \cos(\omega_\mathrm{d} t) + \frac{\zeta}{\sqrt{1-\zeta^2}}\sin(\omega_\mathrm{d} t) & \frac{1}{\omega_\mathrm{d}}\sin(\omega_\mathrm{d} t) \\ \frac{-\omega_\mathrm{d}}{\sqrt{1-\zeta^2}}\sin(\omega_\mathrm{d} t) & \cos(\omega_\mathrm{d} t) - \frac{\zeta}{\sqrt{1-\zeta^2}}\sin(\omega_\mathrm{d} t) \end{bmatrix}, & 0 < \zeta < 1 \\ e^{-\zeta\omega t}\begin{bmatrix} 1+\omega t & t \\ -\omega^2 t & 1-\omega t \end{bmatrix}, & \zeta = 1 \\ e^{-\zeta\omega t}\begin{bmatrix} \cosh(\omega_\mathrm{d} t) + \frac{\zeta}{\sqrt{\zeta^2-1}}\sinh(\omega_\mathrm{d} t) & \frac{1}{\omega_\mathrm{d}}\sinh(\omega_\mathrm{d} t) \\ \frac{-\omega_\mathrm{d}}{\sqrt{\zeta^2-1}}\sinh(\omega_\mathrm{d} t) & \cosh(\omega_\mathrm{d} t) - \frac{\zeta}{\sqrt{\zeta^2-1}}\sinh(\omega_\mathrm{d} t) \end{bmatrix}, & \zeta > 1 \end{cases} \tag{27}$$

Fig. 4 presents $e^{\eta(\zeta)} = \omega\, g_{\max}/\dot{g}(t_0)$ as a function of ζ for $0 < \zeta \leqslant 5$ subject to Case 2 initial conditions. When the agents are given, the maximum agent speeds are fixed; thus, $\dot{g}(t_0)$ is upper bounded. Therefore, $g_{\max}$ can be reduced by increasing ζ and/or ω.

The control design is specified by R, d, ζ, and ω such that the multiagent system is compact within a radius-R circle centered at the virtual leader, with the constraint violations quickly stabilized and the worst-case collisions less than the buffer size d, subject to the agent actuator dynamics and saturation.

F. Actuator Saturation and Dynamics

To add important realism to our formulation, we assume that the actuator is subject to saturation limits

$$\mathbf{f}_{\rm cmd} = \min\{\, \max\{-\mathbf{A}^{\mathsf{T}}\boldsymbol{\lambda},\ \mathbf{f}_{\rm lbd}\},\ \mathbf{f}_{\rm ubd}\,\} \tag{30}$$

and first-order dynamics

$$\dot{\mathbf{f}}_{\rm act} = \frac{1}{\tau}(\mathbf{f}_{\rm cmd} - \mathbf{f}_{\rm act}) \tag{31}$$

where $\mathbf{f}_{\rm lbd} \in \mathbb{R}^{2N}$ and $\mathbf{f}_{\rm ubd} \in \mathbb{R}^{2N}$ are the lower and upper bounds for command control force, respectively, $\mathbf{f}_{\rm cmd} \in \mathbb{R}^{2N}$ is the saturated command control force, $\mathbf{f}_{\rm act} \in \mathbb{R}^{2N}$ is the actual control force, and $0.05\ \text{s} \lessapprox \tau \lessapprox 1.0\ \text{s}$ is a time constant. Note that $\dot{\mathbf{f}}_{\rm act}$ is bounded automatically under the initial conditions $\mathbf{f}_{\rm act}(t=0) = \mathbf{0}$.

With the saturated and delayed actuator force $\mathbf{f}_{\rm act}$, the actual acceleration is recomputed by $\hat{\ddot{\mathbf{q}}} = \mathbf{M}^{-1}(\mathbf{f} + \mathbf{f}_{\rm act})$. The state derivative vector $[\dot{\mathbf{q}}^{\mathsf{T}}\ \ \hat{\ddot{\mathbf{q}}}^{\mathsf{T}}\ \ \dot{\mathbf{f}}_{\rm act}^{\mathsf{T}}]^{\mathsf{T}}$ is then used in the numerical integration.

IV. Rank Deficient KKT Systems

Denoting $C = n_{\rm f} + n_{\rm c}$ as the total number of active constraints at the present time step, (24) can be rewritten as

$$\begin{bmatrix} \mathbf{M} & \mathbf{A}^{\mathsf{T}} \\ \mathbf{A} & \mathbf{0} \end{bmatrix} \begin{bmatrix} \ddot{\mathbf{q}} \\ \boldsymbol{\lambda} \end{bmatrix} = \begin{bmatrix} \mathbf{f} \\ \hat{\mathbf{b}} \end{bmatrix} \iff \mathbf{H}\mathbf{z} = \mathbf{w} \tag{32}$$

where $\mathbf{A} = [\mathbf{A}_{g_{\rm f}}^{\mathsf{T}}\ \ \mathbf{A}_{g_{\rm c}}^{\mathsf{T}}]^{\mathsf{T}} \in \mathbb{R}^{C\times 2N}$.

It has been proved in Section II-B that the KKT system (32) in this study has a unique solution when $\mathbf{A}$ is full rank. We discuss some scenarios where $\mathbf{A}$ becomes rank deficient.

Lemma 1: Consider an N-agent system with three pairwise colliding agents aligned in a row (as shown in Fig. 5). Then, $\mathbf{A}$ in (32) for this system is rank deficient.

Proof: We consider the N-agent system with three colliding agents as illustrated in Fig. 5. Without loss of generality, we assume that the indices for these three agents are 1, 2, and 3. Then, the three rows of $\mathbf{A}$ that correspond to the three collision avoidance constraints are

$$\begin{bmatrix} -\chi_{12} & -\xi_{12} & \chi_{12} & \xi_{12} & 0 & 0 & \mathbf{0}_{1\times(2N-6)} \\ -\chi_{13} & -\xi_{13} & 0 & 0 & \chi_{13} & \xi_{13} & \mathbf{0}_{1\times(2N-6)} \\ 0 & 0 & -\chi_{23} & -\xi_{23} & \chi_{23} & \xi_{23} & \mathbf{0}_{1\times(2N-6)} \end{bmatrix}. \tag{33}$$

The three agents are distributed along a straight line; thus, $\exists$ a constant $c \neq 0$ such that $c\chi_{12} = \chi_{23}$, $c\xi_{12} = \xi_{23}$. We have $\chi_{13} = \chi_{12} + \chi_{23} = (c+1)\chi_{12} = (c+1)\chi_{23}/c$, $\xi_{13} = \xi_{12} + \xi_{23} = (c+1)\xi_{12} = (c+1)\xi_{23}/c$; hence, in (33), the second row can be expressed as a linear combination of the first and third rows. Therefore, an N-agent system with three pairwise colliding agents aligned in a row has a rank deficient $\mathbf{A}$.

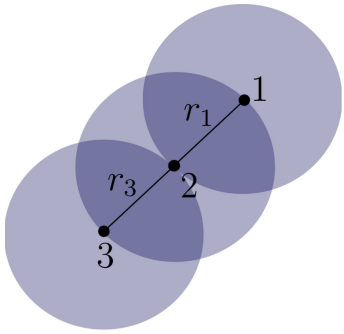

Fig. 5. Three agents aligned in a row with all pairwise collision avoidance constraints violated, resulting in a degenerate $\mathbf{A}$.

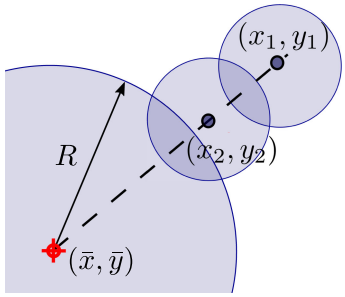

Fig. 6. Two colliding agents aligned with the virtual leader outside the circle R, resulting in a degenerate $\mathbf{A}$.

Lemma 2: Consider an N-agent system with two colliding agents aligned with the virtual leader outside the circle R (as shown in Fig. 6). Then, $\mathbf{A}$ in (32) for this system is rank deficient.

Proof: Without loss of generality, we assume that the leader following constraints for the colliding agent pair $\{1, 2\}$ are violated. Then, the three rows of $\mathbf{A}$ that correspond to the active constraints under this scenario are

$$\begin{bmatrix} \mu_1 & \nu_1 & 0 & 0 & \mathbf{0}_{1\times(2N-4)} \\ 0 & 0 & \mu_2 & \nu_2 & \mathbf{0}_{1\times(2N-4)} \\ -\chi_{12} & -\xi_{12} & \chi_{12} & \xi_{12} & \mathbf{0}_{1\times(2N-4)} \end{bmatrix}. \tag{34}$$

We also assume that agent 1, 2, and the virtual leader are aligned in a line, i.e., $\exists$ two constants $c_1 \neq 0$ and $c_2 \neq 0$ such that $\chi_{12} = c_1\mu_1 = c_2\mu_2$, $\xi_{12} = c_1\nu_1 = c_2\nu_2$. Hence, the third row in (34) can be expressed as a linear combination of the first and second rows, resulting in $\mathbf{A}$ in (32) being rank deficient. ■

Note that when $g_{{\rm f}_i}$, $g_{{\rm f}_j}$, and $g_{{\rm c}_{ij}}$, $\forall i, j \in \{1, 2, \ldots, N\}$, are active, all the symbolic entries in the corresponding rows of $\mathbf{A} \in \mathbb{R}^{C\times 2N}$, μ_i, ν_i, μ_j, ν_j, χ_{ij}, and ξ_{ij}, cannot be all zero, i.e., each row of $\mathbf{A}$ has a nonzero 2-norm.

V. Handling a Rank Deficient Matrix $\mathbf{A}$

In a large-scale multiagent system, degenerate scenarios as stated in Lemmas 1 and 2 are not rare. Benzi *et al.* [47] present an extensive review on methods to solve saddle point problems, in which the constraint matrix is full rank and the mass matrix is semidefinite (a setup different from that in this section). Extending the results in [47], this section compares two QR-based formulations to solving degenerate KKT systems (32) and provides bias error bounds for regularized KKT systems.

For simplicity, we assume a homogeneous N-agent, mass-m system, i.e., $\mathbf{M} = m\mathbf{I}$. Denoting $\text{rank}(\mathbf{A}) = k$, we have $k \leqslant C$.

A. QR Decomposition With Column Pivoting (QRP)

The QRP algorithm [48] factorizes a matrix into an upper triangular matrix with nonincreasing main diagonal entries.

Our objective is to solve the linear least-squares problem

$$\min_{\ddot{\mathbf{q}},\boldsymbol{\lambda}} \left\| \begin{bmatrix} \mathbf{M} & \mathbf{A}^\intercal \\ \mathbf{A} & \mathbf{0} \end{bmatrix} \begin{bmatrix} \ddot{\mathbf{q}} \\ \boldsymbol{\lambda} \end{bmatrix} - \begin{bmatrix} \mathbf{f} \\ \hat{\mathbf{b}} \end{bmatrix} \right\|_2^2 \triangleq \min_{\ddot{\mathbf{q}},\boldsymbol{\lambda}} \|\mathbf{H}\mathbf{z} - \mathbf{w}\|_2^2 \,. \quad (35)$$

1) Apply QRP to $\mathbf{H}$: When the square matrix $\mathbf{H}$ is not full rank, we have

$$\mathbf{H} = \mathbf{Q}\mathbf{R}\mathbf{P}^\intercal = \begin{bmatrix} \mathbf{Q}_1 & \mathbf{Q}_2 \end{bmatrix} \begin{bmatrix} \mathbf{R}_1 & \mathbf{R}_2 \\ \mathbf{0} & \mathbf{0} \end{bmatrix} \begin{bmatrix} \mathbf{P}_1^\intercal \\ \mathbf{P}_2^\intercal \end{bmatrix} \quad (36)$$

where $\text{rank}(\mathbf{H}) = 2N + k$, the columns of both $\mathbf{Q}_1 \in \mathbb{R}^{(2N+C)\times(2N+k)}$ and $\mathbf{Q}_2 \in \mathbb{R}^{(2N+C)\times(C-k)}$ are orthonormal, $\mathbf{R}_1 \in \mathbb{R}^{(2N+k)\times(2N+k)}$ is a nonsingular upper triangular matrix with nonincreasing main diagonal entries, $\mathbf{R}_2 \in \mathbb{R}^{(2N+k)\times(C-k)}$ is a rectangular matrix with each column lying in the range of $\mathbf{R}_1$, and both $\mathbf{P}_1^\intercal \in \mathbb{R}^{(2N+k)\times(2N+C)}$ and $\mathbf{P}_2^\intercal \in \mathbb{R}^{(C-k)\times(2N+C)}$ have orthonormal columns. Therefore,

$$\mathbf{H}\mathbf{z} = \mathbf{H}\mathbf{P}\mathbf{P}^\intercal\mathbf{z} = \begin{bmatrix} \mathbf{Q}_1\mathbf{R}_1 & \mathbf{Q}_1\mathbf{R}_2 \end{bmatrix} \begin{bmatrix} \mathbf{P}_1^\intercal \\ \mathbf{P}_2^\intercal \end{bmatrix} \mathbf{z} = \mathbf{w} \,. \quad (37)$$

In (37), $\mathbf{P}_2^\intercal\mathbf{z}$ corresponds to $\mathbf{Q}_1\mathbf{R}_2$ whose columns are linearly dependent on the columns of $\mathbf{Q}_1\mathbf{R}_1$. Setting $\mathbf{P}_2^\intercal\mathbf{z}$ in (37) to zero, we have

$$\mathbf{Q}_1\mathbf{R}_1\mathbf{z}_1 = \mathbf{w} \quad (38)$$

where $\mathbf{z}_1 = \mathbf{P}_1^\intercal\mathbf{z} \in \mathbb{R}^{2N+k}$ contains the constrained accelerations and Lagrange multipliers corresponding to $(2N + k)$ linearly independent columns $\mathbf{Q}_1\mathbf{R}_1$.

Due to the partition of $\mathbf{P}$, the right $C - k$ columns of $\mathbf{P}_1^\intercal$ are full of zeros, thus making $\mathbf{Q}_1\mathbf{R}_1\mathbf{P}_1^\intercal$ rank deficient. This means that although $\mathbf{Q}_1\mathbf{R}_1\mathbf{P}_1^\intercal$ has the same dimension as that of $\mathbf{H}$, $\mathbf{z}$ cannot be uniquely determined.

Note that $\mathbf{Q}_1\mathbf{R}_1$ is a tall rectangular matrix of full rank; thus, (38) is an overdetermined system. Hence, a linear least-squares approximation of $\mathbf{z}_1$ can be obtained by solving the normal equations of (38).

2) Apply QRP to $\mathbf{A}^\intercal$: Applying QRP algorithm [48] to $\mathbf{A}^\intercal$ when $\mathbf{A}$ is not full rank, we have

$$\mathbf{A}^\intercal = \mathbf{Q}\mathbf{R}\mathbf{P}^\intercal = \begin{bmatrix} \mathbf{Q}_r & \mathbf{Q}_{\bar{r}} \end{bmatrix} \begin{bmatrix} \mathbf{R}_r & \mathbf{R}_{\bar{r}} \\ \mathbf{0} & \mathbf{0} \end{bmatrix} \begin{bmatrix} \mathbf{P}_r^\intercal \\ \mathbf{P}_{\bar{r}}^\intercal \end{bmatrix} \quad (39)$$

where both $\mathbf{Q}_r \in \mathbb{R}^{2N\times k}$ and $\mathbf{Q}_{\bar{r}} \in \mathbb{R}^{2N\times(2N-k)}$ have orthonormal columns, $\mathbf{R}_r \in \mathbb{R}^{k\times k}$ is a nonsingular upper triangular matrix with nonincreasing main diagonal elements, $\mathbf{R}_{\bar{r}} \in \mathbb{R}^{k\times(C-k)}$ is a rectangular matrix with each column lying in the range of $\mathbf{R}_r$, and the columns of both $\mathbf{P}_r^\intercal \in \mathbb{R}^{k\times C}$ and $\mathbf{P}_{\bar{r}}^\intercal \in \mathbb{R}^{(C-k)\times C}$ are orthonormal vectors.

Hence, (32) is equivalent to

$$\begin{bmatrix} \mathbf{M} & \mathbf{A}^\intercal\mathbf{P} \\ \mathbf{P}^\intercal\mathbf{A} & \mathbf{0} \end{bmatrix} \begin{bmatrix} \ddot{\mathbf{q}} \\ \mathbf{P}^\intercal\boldsymbol{\lambda} \end{bmatrix} = \begin{bmatrix} \mathbf{f} \\ \mathbf{P}^\intercal\hat{\mathbf{b}} \end{bmatrix}$$

$$\iff \begin{bmatrix} \mathbf{M} & \mathbf{Q}_r\mathbf{R}_r & \mathbf{Q}_r\mathbf{R}_{\bar{r}} \\ \mathbf{R}_r^\intercal\mathbf{Q}_r^\intercal & \mathbf{0} & \mathbf{0} \\ \mathbf{R}_{\bar{r}}^\intercal\mathbf{Q}_r^\intercal & \mathbf{0} & \mathbf{0} \end{bmatrix} \begin{bmatrix} \ddot{\mathbf{q}} \\ \mathbf{P}_r^\intercal\boldsymbol{\lambda} \\ \mathbf{P}_{\bar{r}}^\intercal\boldsymbol{\lambda} \end{bmatrix} = \begin{bmatrix} \mathbf{f} \\ \mathbf{P}_r^\intercal\hat{\mathbf{b}} \\ \mathbf{P}_{\bar{r}}^\intercal\hat{\mathbf{b}} \end{bmatrix} \,. \quad (40)$$

In (40), $\mathbf{P}_{\bar{r}}^\intercal\boldsymbol{\lambda}$ corresponds to $\mathbf{Q}_r\mathbf{R}_{\bar{r}}$ whose columns are linearly dependent on those of $\mathbf{Q}_r\mathbf{R}_r$. Setting $\mathbf{P}_{\bar{r}}^\intercal\boldsymbol{\lambda}$ to zero and removing the redundant constraints $\mathbf{R}_{\bar{r}}^\intercal\mathbf{Q}_r^\intercal\ddot{\mathbf{q}} = \mathbf{P}_{\bar{r}}^\intercal\hat{\mathbf{b}}$, we have

$$\begin{bmatrix} \mathbf{M} & \mathbf{Q}_r\mathbf{R}_r \\ \mathbf{R}_r^\intercal\mathbf{Q}_r^\intercal & \mathbf{0} \end{bmatrix} \begin{bmatrix} \ddot{\mathbf{q}} \\ \mathbf{P}_r^\intercal\boldsymbol{\lambda} \end{bmatrix} = \begin{bmatrix} \mathbf{f} \\ \mathbf{P}_r^\intercal\hat{\mathbf{b}} \end{bmatrix} \,. \quad (41)$$

Note that the coefficient matrix in (41) is square and full rank. Therefore, the unknowns in (41), $\ddot{\mathbf{q}}$ and $\mathbf{P}_r^\intercal\boldsymbol{\lambda}$, and thus the command control forces, $-\mathbf{Q}_r\mathbf{R}_r\mathbf{P}_r^\intercal\boldsymbol{\lambda}$, can be uniquely determined.

3) Conclusion: From the derivations and discussions in Sections V-A1 and V-A2, we can conclude that applying QRP to $\mathbf{A}^\intercal$ is superior to applying QRP to $\mathbf{H}$ due to the guaranteed uniqueness of solution and a cheaper computational cost (applying QRP to a matrix of a smaller size).

B. Regularization

The minimization problem (15) may be regularized as

$$\max_{\boldsymbol{\lambda}} \min_{\ddot{\mathbf{q}}} \frac{1}{2}(\ddot{\mathbf{q}} - \mathbf{a})^\intercal\mathbf{M}(\ddot{\mathbf{q}} - \mathbf{a}) + \boldsymbol{\lambda}^\intercal(\mathbf{A}\ddot{\mathbf{q}} - \hat{\mathbf{b}}) - \frac{\beta}{2}\boldsymbol{\lambda}^\intercal\boldsymbol{\lambda} \quad (42)$$

where $0 < \beta \ll m$ is the regularization factor, and $\beta = 0$ yields the original problem.

Note that the regularized Lagrangian (42) is still convex and thus has a unique solution that satisfies the KKT conditions

$$\begin{bmatrix} \mathbf{M} & \mathbf{A}^\intercal \\ \mathbf{A} & -\beta\mathbf{I} \end{bmatrix} \begin{bmatrix} \ddot{\mathbf{q}} \\ \boldsymbol{\lambda} \end{bmatrix} = \begin{bmatrix} \mathbf{f} \\ \hat{\mathbf{b}} \end{bmatrix} \iff \widetilde{\mathbf{H}}\tilde{\mathbf{z}} = \mathbf{w} \quad (43)$$

where $\tilde{\mathbf{z}}$ is the unique approximation of the solution to the original constrained minimization problem (16).

1) Error Analysis of Regularization: We have the original and regularized KKT systems

$$\begin{aligned} \mathbf{H}\mathbf{z} &= \mathbf{w} \\ \widetilde{\mathbf{H}}\tilde{\mathbf{z}} &= \mathbf{w} \,. \end{aligned} \quad (44)$$

Note that the regularized KKT matrix $\widetilde{\mathbf{H}}$ is nonsingular whether $\mathbf{A}$ is full rank or not. Thus, we may compute the bias error due to regularization as

$$\begin{aligned} \tilde{\mathbf{z}} - \mathbf{z} &= \widetilde{\mathbf{H}}^{-1}\mathbf{w} - \mathbf{z} = \widetilde{\mathbf{H}}^{-1}\mathbf{H}\mathbf{z} - \mathbf{z} \\ &= \widetilde{\mathbf{H}}^{-1}(\widetilde{\mathbf{H}} - \mathbf{S}_1)\mathbf{z} - \mathbf{z} = \mathbf{z} - \widetilde{\mathbf{H}}^{-1}\mathbf{S}_1\mathbf{z} - \mathbf{z} \\ &= -\widetilde{\mathbf{H}}^{-1}\mathbf{S}_1\mathbf{z} \end{aligned} \quad (45)$$

TABLE I
TWO TYPES OF INITIAL CONDITIONS FOR TWO AGENTS SUBJECT ONLY TO COLLISION AVOIDANCE CONSTRAINT

Variables	Case-1-type (C1)	Case-2-type (C2)
$\mathbf{p}_1(0)$	$(-2, 0)$	$(-10, 0)$
$\mathbf{p}_2(0)$	$(2, 0)$	$(10, 0)$
$\mathbf{v}_1(0)$	$(0, 0)$	$(10, 0)$
$\mathbf{v}_2(0)$	$(0, 0)$	$(-10, 0)$
$g_{c_{12}}(0)$	240	0
$\dot{g}_{c_{12}}(0)$	0	640

where

$$\mathbf{S}_1 = \widetilde{\mathbf{H}} - \mathbf{H} = \begin{bmatrix} \mathbf{0} & \mathbf{0} \\ \mathbf{0} & -\beta\mathbf{I} \end{bmatrix}.$$

Therefore, the relative error for the solution $\mathbf{z} = [\ddot{\mathbf{q}}^\mathsf{T} \quad \boldsymbol{\lambda}^\mathsf{T}]^\mathsf{T}$ due to regularization can be computed in terms of Frobenius norms

$$\frac{\|\tilde{\mathbf{z}} - \mathbf{z}\|_\mathrm{F}}{\|\mathbf{z}\|_\mathrm{F}} \leqslant \|\widetilde{\mathbf{H}}^{-1}\mathbf{S}_1\|_\mathrm{F} \leqslant \|\widetilde{\mathbf{H}}^{-1}\|_\mathrm{F} \cdot \|\mathbf{S}_1\|_\mathrm{F} = \beta\sqrt{C}\|\widetilde{\mathbf{H}}^{-1}\|_\mathrm{F} \tag{46}$$

where the Cauchy-Schwarz inequality is applied.

Thus, the degeneracy issue of the original KKT system can be resolved by the introduced regularization approach.

Due to the asymptotic convergence of constraint errors, the symbolic entries of $\mathbf{A}$ are finite at all times. However, note that $\mathbf{A}$ is problem-dependent and time-dependent; thus, we cannot specify a universal upper bound for the Frobenius norm of the relative bias error in (46).

VI. EXAMPLES AND DISCUSSIONS

A. Head-On Collision Subject to Maximum Speed

In order to examine the performance of the proposed control law in a worst-case collision scenario, we study the responses of two agents heading toward each other subject to only collision avoidance constraint, $g_{c_{12}}$. Assume that there is no nonconstraint force. The agents' masses are $m_1 = m_2 = 10$ kg, the safety distance is 16 m, the natural frequency ω_c is fixed at 5 rad/s in all cases, and the damping ratio ζ_c is respectively assigned 0.5 and 1.5 for both types of initial conditions for constraint dynamics, as introduced in Section III-E. The constant time step for numerical integration is 0.005 s, where fourth-order Runge-Kutta method is used.

Two types of initial conditions (at $t = 0$), the position vectors $\mathbf{p}(t)$ and the velocity vectors $\mathbf{v}(t)$, for agents 1 and 2 are given in Table I. Note that Case-2-type (C2) initial conditions correspond to a scenario where both agents are subject only to head-on collision under maximum speed.

Note that for two underdamped cases, the second-order analytical response of constraint violation oscillates between positive and negative values. Hence, values below zero are truncated for analytical solutions since the control actions are enforced only when the corresponding constraint value becomes positive. Agents continue moving away from each other at constant speeds once the collision avoidance constraint becomes inactive.

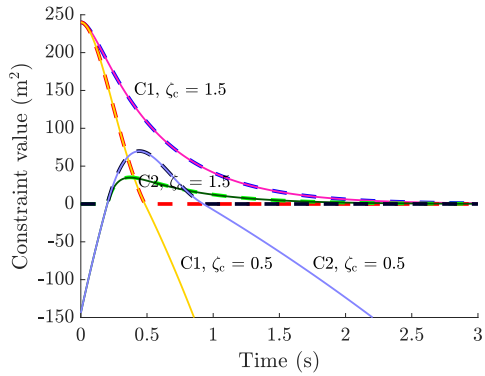

Fig. 7. Numerical vs. analytical solutions of the collision avoidance constraint values for agents 1 and 2, subject to two types of initial conditions for $g_{c_{12}}$ and different damping ratios. $\omega_c = 5$ rad/s in all four cases. The dashed lines denote analytical solutions, and the solid lines denote numerical solutions. The initial conditions for Case-1-type (C1) and for Case-2-type (C2) are given in Table I. All analytical solutions only keep the positive values for $g_{c_{12}}$ since the second-order constraint stabilizer (12) is enforced only when the constraint is active. The numerical solution agrees well with the analytical solution for all four cases.

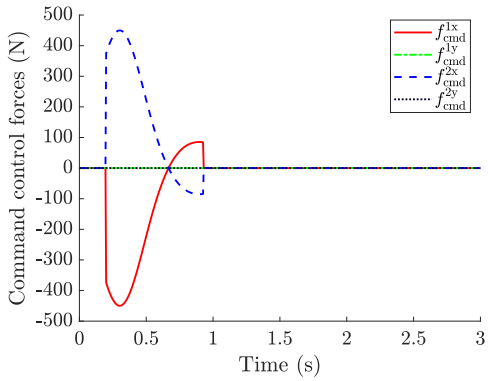

Fig. 8. Components of the command control forces $\mathbf{f}_{\mathrm{cmd}} = -\mathbf{A}^\mathsf{T}\boldsymbol{\lambda}$ for two-agent head-on collision-only case subject to maximum speed for the C2 initial conditions and $\zeta_c = 0.5$ in Fig. 7. The Y components of $\mathbf{f}_{\mathrm{cmd}}$, f_{cmd}^{1y} and f_{cmd}^{2y}, are zero for all time. It is evident that the overall command controls are nonlinear and discontinuous.

Fig. 7 demonstrates the agreement between the analytical and numerical solutions for constraint dynamics and the guaranteed safety under this worst-case collision scenario for the agents' characteristic length $l_1 = l_2 = 4$ m. For both types of initial conditions and for both underdamped and overdamped ζ_c, the active constraint dynamics follow an analytical second-order oscillator, and the constraint error asymptotically goes arbitrarily small. This proves the asymptotic convergent behavior of the proposed controller and thus provides a guarantee for strict collision prevention between agents, under properly selected, problem-dependent control parameters.

The components of the command control forces of the two agents for C2 initial conditions and $\zeta_c = 0.5$ are shown in Fig. 8. It is evident that the overall command control actions $-\mathbf{A}^\mathsf{T}\boldsymbol{\lambda}$ are nonlinear and discontinuous and that the X components of $-\mathbf{A}^\mathsf{T}\boldsymbol{\lambda}$ have the same magnitude but opposite sign for both agents.

TABLE II
PARAMETERS INVOLVED IN A MULTIAGENT SYSTEM SUBJECT TO ONLY COLLISION AVOIDANCE CONSTRAINTS

Quantities	Variables	Units	Dimensions
Mass	m	kg	$FL^{-1}T^2$
Maximum speed	$V_{\max}$	m/s	LT^{-1}
Length of agent	l	m	L
Safety length ratio	$\alpha \triangleq d_{ij}/l$	1	1
Controls	$-\mathbf{A}^{\mathrm{T}}\boldsymbol{\lambda}$	N	F
Damping ratio	ζ	1	1
Natural frequency	ω	1/s	T^{-1}

B. Dimensional Analysis of Collision Avoidance Constraint

For multiagent systems subject to only collision avoidance constraints, the involved parameters and the corresponding units of dimension are presented in Table II. Table II indicates that seven physical variables and three fundamental dimensions (force F, length L, and time T) are involved in the multiagent head-on collision avoidance problem. Note that damping ratio and safety length ratio are already dimensionless. Thus, according to Buckingham's Pi theorem [49], we have $7-3-2=2$ Pi groups. The four dimensionless groups of the system can be chosen as ζ, α, $\omega l/V_{\max}$, and $\max_t \|\mathbf{A}(t)^{\mathrm{T}}\boldsymbol{\lambda}(t)\|_1 \cdot l/(mV_{\max}^2)$.

The metric of checking collision in a multiagent system is that the minimum pairwise distance between agents $d_{\min}(t)$ is greater than the characteristic length of an agent l at all times (assuming homogeneous multiagent systems)

$$\begin{aligned} \Upsilon_{\mathrm{c}}(t) &\triangleq \min_{i,j}\{\, d_{ij}^2 - g_{\mathrm{c}_{ij}}(t)\,\} \\ d_{\min}(t) &\triangleq \operatorname{sgn}(\Upsilon_{\mathrm{c}}(t)) \cdot \sqrt{|\Upsilon_{\mathrm{c}}(t)|} > l\,,\ \forall\, t \end{aligned} \tag{47}$$

where $\operatorname{sgn}(\cdot)$ denotes the sign function, and the agent indices $\{i,j\}$ become $\{1,2\}$ in a two-agent collision-only scenario.

Given the mass, maximum speed, and agent length of a multiagent system, we can find a set of control parameters that guarantees actual collision avoidance by the dimensional study.

We apply the result to the head-on colliding agent pair in Section VI-A, i.e., $m_1 = m_2 = 10$ kg and $V_{\max} = 10$ m/s, subject to the C2 initial conditions in Table I. One hundred and one samples between 0 and 10 and 101 samples between 0 and 5 are drawn uniformly for ω_{c} and ζ_{c}, respectively. The contour plot of $\max_t \|\mathbf{A}(t)^{\mathrm{T}}\boldsymbol{\lambda}(t)\|_1 \cdot l/(mV_{\max}^2)$ are then plotted based on these 101×101 grids. The simulation time window is 5 s for each run, which is long enough for $g_{\mathrm{c}_{12}}$ to achieve peak response.

Fig. 9 provides the information required for choosing proper control parameters for a given multiagent system. It indicates that in order to account for control saturation and to guarantee no actual collisions, ζ and ω need to be selected such that the resulting nondimensional maximum control action is close to the right of the l-level contour (in this case, $l_1 = l_2 = 4$ m), which is the boundary between collision and no-collision regions. Furthermore, the selected ζ and ω should not be too large.

Fig. 10 presents the l-level contours for different values of l. Each l-level contour is obtained based on a same set of 101×101 grids as those of Fig. 9. It indicates that as the agent size increases, the chosen ζ and/or ω also increase in order to guarantee no actual collision between agents.

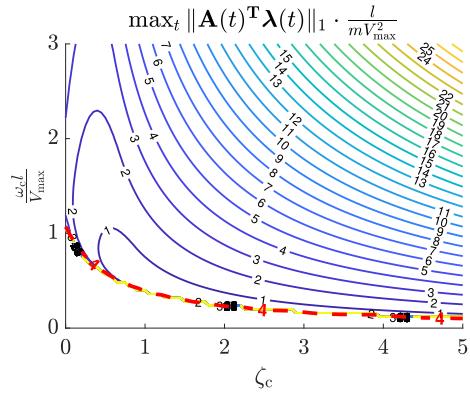

Fig. 9. Contours of nondimensional maximum control action for the two-agent head-on maximum-speed collision in Section VI-A. The contours are based on 101×101 uniform grids. The labels for solid contour lines denote the dimensionless maximum control forces over time. The red dashed line denotes the l-level contour, which signals whether real collision occurs between the agents or not. The region to the upper right of the l-level contour is the admissible region where no actual collision happens.

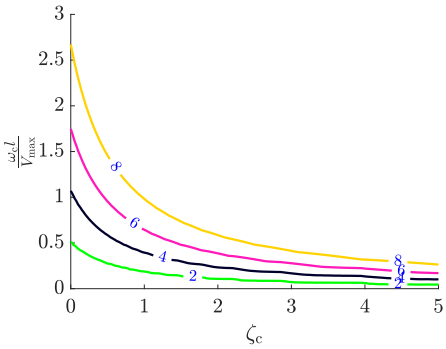

Fig. 10. l-level contours given different values of $\alpha \triangleq d_{12}/l$ for the two-agent head-on maximum-speed collision in Section VI-A. l-level contours represent critical pairwise distance that no actual collision occurs. The contour labels denote the numeric values of l.

C. Swarm Navigation

In this section, we simulate a swarm of 100 homogeneous agents to follow a prescribed virtual leader based on the proposed framework. In this and the next section, the simulations are conducted in MATLAB using fourth-order Runge-Kutta method as the numerical integrator with a constant time step of 0.005 s. For all the presented simulations, the virtual leader to be followed remains stationary during the first and last 5 s of the simulation time window. The swarm has $m_i = 10$ kg and zero initial velocities for agent $i, \forall i$, while the X and Y initial positions for all agents (shown in Fig. 11) are respectively generated from a sequence of uniformly distributed random numbers in the interval $[-110,\ 110]$ m and are labeled into four groups by the k-means++ algorithm [50] using four distinct colors for better visualization purpose. Actuator forces are subject to a

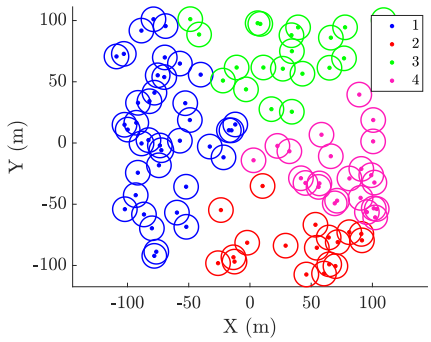

Fig. 11. Random initial positions for 100 agents labeled into four groups by the k-means++ algorithm [50]. The random numbers follow a uniform distribution between -110 and 110 m in both directions. Observe that some agent pairs have buffers overlapped at $t = 0$, indicating an inadmissible initial configuration space.

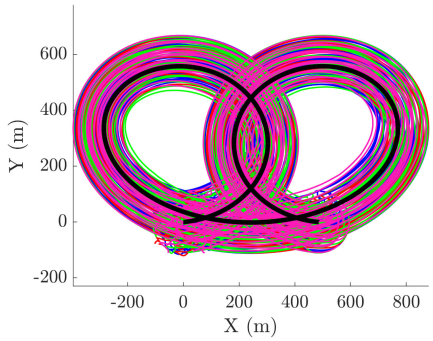

Fig. 12. Trajectories of 100 agents (labeled into four groups) following a virtual leader, whose prescribed trajectory is shown as the black solid line (approximately 4000 m in length).

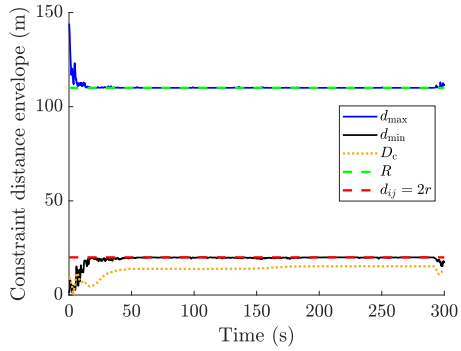

Fig. 13. Time series of the maximum agent-leader distance, $d_{\max}$, the minimum agent-agent distance, $d_{\min}$, and the swarm-centroid-leader distance, D_c, compared to swarm radius R and safety buffer size d_{ij}. Space beneath the green dash line and above the red dash line are the admissible space for the leader following constraint and the collision avoidance constraint, respectively.

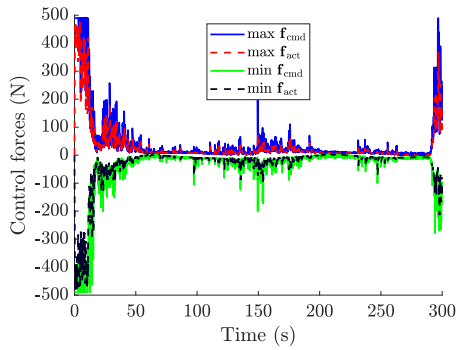

Fig. 14. Time series of the extreme values of the command control forces $\mathbf{f}_{\text{cmd}}$ and the actual control forces $\mathbf{f}_{\text{act}}$.

saturation limit of $5m_ig$ N and respond to commands with a first-order delay constant of 0.2 s, where $g = 9.8$ m/s^2 is the gravitational acceleration. For computation efficiency purpose, regularization is employed in solving the possibly degenerate KKT system with a regularization factor $\beta = 10^{-4}m_i$. Note that the exogenous forces are assumed to be zero for all agents.

The control parameters in the proposed model are selected as $R = 110$ m, $d_{ij} = r_i + r_j = 2r = 20$ m, $\omega_{\text{f}} = \omega_{\text{c}} = 2$ rad/s, and $\zeta_{\text{f}} = \zeta_{\text{c}} = 1$. The trajectories for 100 agents tracing a virtual leader are presented in Fig. 12, where the corresponding animation can be found online.[1]

Due to the implemented Baumgarte's stabilization, both the maximum agent-leader distance $d_{\max}(t)$ and the minimum pairwise distance $d_{\min}(t)$ have the tendency to asymptotically converge from the inadmissible space to the admissible space at any instant of time as shown in Fig. 13, where

$$\Upsilon_{\text{f}}(t) \triangleq \max_i \{\, g_{\text{f}_i}(t) + R^2 \,\}$$

$$d_{\max}(t) \triangleq \text{sgn}(\Upsilon_{\text{f}}(t)) \cdot \sqrt{|\Upsilon_{\text{f}}(t)|}\,, \quad \forall t\,.$$

When a constraint becomes inactive, it does not contribute to the control actions on any agent.

[1][Online]. Available: https://youtu.be/HkIxFIba1sI

We may observe from Figs. 12 and 13 that the swarm smoothly transports without actual interagent collisions, with an almost compact shape except the initial adjusting stage and the final braking stage. This can also be evidenced in Fig. 13 by the relatively stable curves of $d_{\max}$, $d_{\min}$, and D_c except both ends, and in Fig. 14 by the relatively small extreme control forces during the transition and by nearly saturated control forces at the start and increased control forces at the end. At the initial and final phases of the transition, the virtual leader undergoes a sudden change in velocity, and the positions of the agents are more random than those during navigation, when the virtual leader is moving with continuous velocity and the swarm is navigating in a roughly compact shape. Hence, both active leader following and collision avoidance constraints are enforced to the admissible spaces more quickly and drastically at the initial and final stages than those during navigation. This explains the control forces having higher frequencies and higher magnitudes at both ends than those in the intermediate stage.

Of the two types of constraints considered in the multiagent swarming problem, the collision avoidance constraint is more critical, as it dictates the safety of the system. By allowing the violation of hard constraints (colliding buffers among agents), we reduce the magnitudes of the required control actions while ensuring no actual collisions among agents. (The minimum

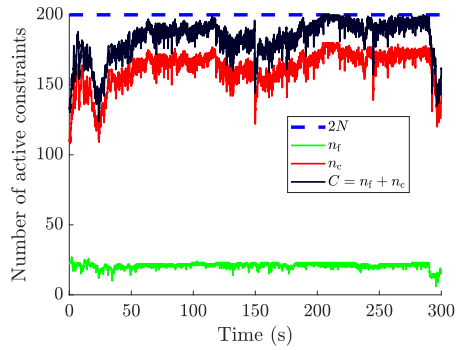

Fig. 15. Number of the active constraints over time.

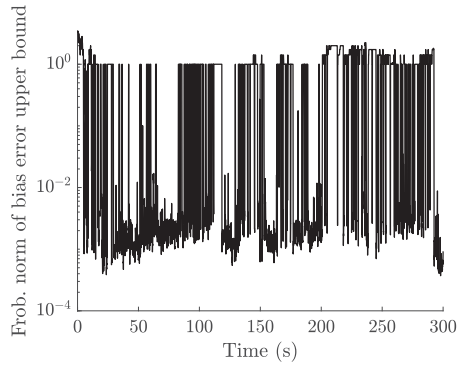

Fig. 16. Time series of the Frobenius norm of the upper bound for the relative bias error due to regularization.

pairwise distance among agents are lower bounded by the buffer size and thus the characteristic length of an agent, as seen in Fig. 13.)

Fig. 15 illustrates that during the most part of the swarming, the number of active leader following constraints n_f remains approximately stable, while the number of active collision avoidance constraints n_c is dynamically changing over time, revealing the highly nonlinear and dynamical nature of the problem.

From Fig. 16, we may observe that the Frobenius norm of the upper bound for the relative bias error has a relatively small magnitude (approximately 10^{-3}) during most part of the swarming and that it becomes significant at the initial organizing stage and reaches spikes with magnitudes of around 1 at some time instants during the transition. As discussed earlier in Section V-B, it is not possible to specify the upper bound norm of the relative bias error at all times due to the problem-dependent and time-dependent nature of $\mathbf{A}$. Furthermore, a large upper bound for the relative bias error does not necessarily indicate a large bias error. Since the swarm possesses a compact shape, the agents execute smooth motion trajectories, the actual control actions are not saturated, and the constraint violations are consistently stabilized to the admissible spaces, we may safely conclude that the bias error is reasonably small during the swarm navigation.

D. Computational Complexity and Solver Details

The computational complexity of the proposed approach for controlling a multiagent system with collision avoidance is determined mainly by two factors: the number of agents N and the number of active constraints C. For multiagent systems discussed herein, there are $2N$ decision variables that contain $\mathbf{f}_{\text{cmd}}$ in (30), up to order-N active leader following constraints, and up to order-N active collision avoidance constraints, as evidenced from Fig. 15.

TABLE III
COMPUTATION TIME PER ITERATION (MILLISECOND) FOR MULTIAGENT SYSTEMS WITH DIFFERENT NUMBERS OF AGENTS AND RANDOM INITIAL POSITIONS

$N = 5$	$N = 10$	$N = 20$	$N = 40$
0.0561	0.0894	0.176	0.443
$N = 50$	$N = 60$	$N = 80$	$N = 100$
0.680	0.990	1.927	3.620

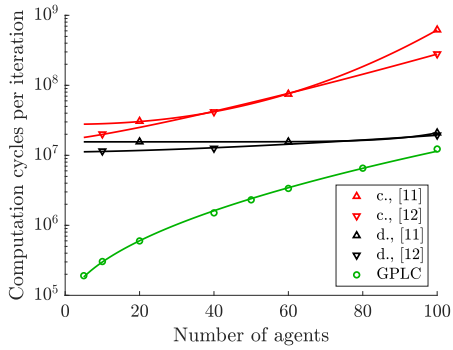

Fig. 17. Comparison of computation cycles per iteration between the GPLC control and the controllers proposed in [11] and [12]. The legends c. and d. are abbreviated for centralized and decentralized, respectively. The computation cycles per iteration is calculated by multiplying the computation time per iteration with the corresponding processor's clock rate. The data points are fitted by power laws.

Table III presents the elapsed real computation time per iteration for multiagent systems as that in Section VI-C. The numerical simulations are conducted in MATLAB on a Windows desktop with a 3.40-GHz Intel i5-7500 processor and 8-GB memory. The only two differences in the simulation setup between these runs are the number of agents and the randomly generated X and Y initial positions for all agents that respectively follow a uniform distribution within a same range.

The elapsed real-time calculation considers the time accumulated over the 300-s simulation window that is spent on identifying active constraints, on constructing and solving the KKT system (43), and on computing and saturating the command control actions. Then, the computation time per time step is obtained by dividing the total accumulative elapsed real-time by the total number of integration steps.

Fig. 17 demonstrates how the computation cycles per time step of the entire GPLC method scales with the number of agents in comparison to existing centralized and decentralized methods [11], [12]. Note that different problems are presented in [11] and [12] from the problem presented in Section VI-C and that the computation times presented in [11] and [12] pertain only to the computation of the safety barrier certificates, which analogously are the collision avoidance constraints on the

command control actions in our approach. Our method turns out to be computationally efficient for up to at least 100 agents.

Note that the computation time is affected by initial conditions and control parameters. A set of the inputs that leads to less constraint violations and smoother trajectories would result in a shorter computation time due to the smaller size of $\mathbf{A}$ and $\hat{\mathbf{b}}$ when constructing the KKT system (43) and thus a less computational effort.

VII. Conclusion and Future Work

In this article, a nonlinear and discontinuous feedback control framework is proposed for a 2-D multiagent system based on the novel extension of GPLC. To the best of our knowledge, this is the first article that generalizes GPLC for problems with dynamic inequality constraints which are intentionally allowed to be violated. The control actions result purely from the evolution of the constrained system dynamics. Two types of constraints are considered for a multiagent swarm navigation problem: leader following constraint and collision avoidance constraint, which achieve leader following, swarm compactness, and collision avoidance behaviors. The active constraint set is the set of constraints in violation at each point in time. These constraints are stabilized by second-order Baumgarte's error stabilization. A proof is provided for the existence and uniqueness of the solution to the associated KKT system. Specialized solutions to rank deficient KKT systems involving QR decomposition and regularization are also presented. The proposed method guarantees collision avoidance under specified worst-case scenarios and is verified by a dimensional analysis for a given multiagent system. The method is employed in guiding a multiagent swarm up to 100 agents to follow a virtual leader that has a prescribed loop trajectory. Satisfactory simulation results are obtained, demonstrating the efficacy and efficiency of the proposed approach.

Future work along this promising method includes a risk-based sensitivity study of the swarm's tracking performance, occurrence of collisions, and computational complexity upon the Baumgarte coefficients, the number of agents, and the leader velocity, in the context of modeling errors and exogenous disturbances. The proposed scheme can be enhanced by incorporating nonlinear underactuated vehicle dynamics (e.g., autonomous vehicles, unmanned quadrotor drones, unmanned submersibles, etc.) and can be further developed by guiding multiple large-scale multiagent systems to follow intersecting high-curvature paths at high speeds. Last but not least, the proposed approach can be experimentally validated by real-time implementations on a multiagent swarm, thanks to its inherent mathematical simplicity and computational efficiency.

Acknowledgment

The authors would like to thank the anonymous reviewers for providing invaluable comments.

References

[1] R. M. Murray, "Recent research in cooperative control of multivehicle systems," *J. Dyn. Syst., Meas., Control*, vol. 129, no. 5, pp. 571–583, 2007.

[2] M. Brambilla, E. Ferrante, M. Birattari, and M. Dorigo, "Swarm robotics: A review from the swarm engineering perspective," *Swarm Intell.*, vol. 7, no. 1, pp. 1–41, 2013.

[3] M. Hoy, A. S. Matveev, and A. V. Savkin, "Algorithms for collision-free navigation of mobile robots in complex cluttered environments: A survey," *Robotica*, vol. 33, no. 3, pp. 463–497, 2015.

[4] F. Rossi, S. Bandyopadhyay, M. Wolf, and M. Pavone, "Review of multi-agent algorithms for collective behavior: A structural taxonomy," 2018, *arXiv:1803.05464*.

[5] S.-J. Chung, A. A. Paranjape, P. Dames, S. Shen, and V. Kumar, "A survey on aerial swarm robotics," *IEEE Trans. Robot.*, vol. 34, no. 4, pp. 837–855, Aug. 2018.

[6] J. Nocedal and S. Wright, *Numerical Optimization*. Berlin, Germany: Springer Science and Business Media, 2006.

[7] S. Boyd and L. Vandenberghe, *Convex Optimization*. Cambridge, U.K.: Cambridge University Press, 2004.

[8] S. Tang and V. Kumar, "Safe and complete trajectory generation for robot teams with higher-order dynamics," in *Proc. IEEE/RSJ Int. Conf. Intell. Robots Syst.*, 2016, pp. 1894–1901.

[9] F. Augugliaro, A. P. Schoellig, and R. D'Andrea, "Generation of collision-free trajectories for a quadrocopter fleet: A sequential convex programming approach," in *Proc. IEEE/RSJ Int. Conf. Intell. Robots Syst.*, 2012, pp. 1917–1922.

[10] U. Borrmann, L. Wang, A. D. Ames, and M. Egerstedt, "Control barrier certificates for safe swarm behavior," *IFAC-PapersOnLine*, vol. 48, no. 27, pp. 68–73, 2015.

[11] L. Wang, A. D. Ames, and M. Egerstedt, "Safety barrier certificates for collisions-free multirobot systems," *IEEE Trans. Robot.*, vol. 33, no. 3, pp. 661–674, Jun. 2017.

[12] D. Pickem *et al.*, "The robotarium: A remotely accessible swarm robotics research testbed," in *Proc. IEEE Int. Conf. Robot. Autom.*, 2017, pp. 1699–1706.

[13] F. Gao and S. Shen, "Quadrotor trajectory generation in dynamic environments using semi-definite relaxation on nonconvex QCQP," in *Proc. IEEE Int. Conf. Robot. Autom.*, 2017, pp. 6354–6361.

[14] T. Schouwenaars, B. De Moor, E. Feron, and J. How, "Mixed integer programming for multi-vehicle path planning," in *Proc. Eur. Control Conf.*, 2001, pp. 2603–2608.

[15] D. Mellinger, A. Kushleyev, and V. Kumar, "Mixed-integer quadratic program trajectory generation for heterogeneous quadrotor teams," in *Proc. IEEE Int. Conf. Robot. Autom.*, 2012, pp. 477–483.

[16] J. A. Preiss, W. Hönig, N. Ayanian, and G. S. Sukhatme, "Downwash-aware trajectory planning for large quadrotor teams," in *Proc. IEEE/RSJ Int. Conf. Intell. Robots Syst.*, 2017, pp. 250–257.

[17] A. Richards and J. How, "Decentralized model predictive control of cooperating UAVs," in *Proc. 43rd IEEE Conf. Decis. Control*, vol. 4, 2004, pp. 4286–4291.

[18] P. Wang and B. Ding, "A synthesis approach of distributed model predictive control for homogeneous multi-agent system with collision avoidance," *Int. J. Control*, vol. 87, no. 1, pp. 52–63, 2014.

[19] S. Spedicato and G. Notarstefano, "Minimum-time trajectory generation for quadrotors in constrained environments," *IEEE Trans. Control Syst. Technol.*, vol. 26, no. 4, pp. 1335–1344, Jun. 2017.

[20] C. E. Luis and A. P. Schoellig, "Trajectory generation for multiagent point-to-point transitions via distributed model predictive control," *IEEE Robot. Autom. Lett.*, vol. 4, no. 2, pp. 375–382, Apr. 2019.

[21] S. H. Arul and D. Manocha, "DCAD: Decentralized collision avoidance with dynamics constraints for agile quadrotor swarms," *IEEE Robot. Autom. Lett.*, vol. 5, no. 2, pp. 1191–1198, Apr. 2020.

[22] N. E. Leonard and E. Fiorelli, "Virtual leaders, artificial potentials and coordinated control of groups," in *Proc. 40th IEEE Conf. Decis. Control*, vol. 3, 2001, pp. 2968–2973.

[23] M. T. Wolf and J. W. Burdick, "Artificial potential functions for highway driving with collision avoidance," in *Proc. IEEE Int. Conf. Robot. Autom.*, 2008, pp. 3731–3736.

[24] D. V. Dimarogonas and K. J. Kyriakopoulos, "Connectedness preserving distributed swarm aggregation for multiple kinematic robots," *IEEE Trans. Robot.*, vol. 24, no. 5, pp. 1213–1223, Oct. 2008.

[25] S. S. Ge, X. Liu, C.-H. Goh, and L. Xu, "Formation tracking control of multiagents in constrained space," *IEEE Trans. Control Syst. Technol.*, vol. 24, no. 3, pp. 992–1003, May 2016.

[26] J. Zhang, J. Yan, and P. Zhang, "Fixed-wing UAV formation control design with collision avoidance based on an improved artificial potential field," *IEEE Access*, vol. 6, pp. 78342–78351, 2018.

[27] P. Fiorini and Z. Shiller, "Motion planning in dynamic environments using velocity obstacles," *Int. J. Robot. Res.*, vol. 17, no. 7, pp. 760–772, 1998.

[28] J. Van den, M. Berg, Lin, and D., Manocha, "Reciprocal velocity obstacles for real-time multi-agent navigation," in *Proc. IEEE Int. Conf. Robot. Autom.*, 2008, pp. 1928–1935.
[29] J. Van Den, S. J. Berg, M. GuyLin, and D. Manocha, "Reciprocal n-body collision avoidance," in *Robotics Research*. Berlin, Germany: Springer, 2011, pp. 3–19.
[30] J. Van Den Berg, J. Snape, S. J. Guy, and D. Manocha, "Reciprocal collision avoidance with acceleration-velocity obstacles," in *Proc. IEEE Int. Conf. Robot. Autom.*, 2011, pp. 3475–3482.
[31] D. Bareiss and J. van denBerg, "Generalized reciprocal collision avoidance," *Int. J. Robot. Res.*, vol. 34, no. 12, pp. 1501–1514, 2015.
[32] F. E. Udwadia and R. E. Kalaba, "A new perspective on constrained motion," *Proc.: Math. Phys. Sci.*, vol. 439, no. 1906, pp. 407–410, 1992.
[33] C. M. Pappalardo and D. Guida, "Forward and inverse dynamics of a unicycle-like mobile robot," *Machines*, vol. 7, no. 1, 2019, Art. no. 5.
[34] R. Zhao, M. Li, Q. Niu, and Y.-H. Chen, "Udwadia–Kalaba constraint-based tracking control for artificial swarm mechanical systems: Dynamic approach," *Nonlinear Dyn.*, vol. 100, no. 3, pp. 2381–2399, 2020.
[35] C. F. Gauß, "Über ein neues allgemeines grundgesetz der mechanik," *J. Für Die Reine Und Angewandte Mathematik*, vol. 4, pp. 232–235, 1829.
[36] C. Lanczos, *The Variational Principles of Mechanics*, 4th ed. New York, NY, USA: Dover, 1986.
[37] E. T. Whittaker, *A Treatise on the Analytical Dynamics of Particles and Rigid Bodies; With an Introduction to the Problem of Three Bodies*, 4th ed. Cambridge U.K.: Cambridge University Press, 1988.
[38] Y. Liu and R. Bucknall, "A survey of formation control and motion planning of multiple unmanned vehicles," *Robotica*, vol. 36, no. 7, pp. 1019–1047, 2018.
[39] J. Baumgarte, "Stabilization of constraints and integrals of motion in dynamical systems," *Comput. Methods Appl. Mechanics Eng.*, vol. 1, no. 1, pp. 1–16, 1972.
[40] G.-P. Ostermeyer, "On Baumgarte differential algebraic equations," in *Proc. NATO Adv. Res. Workshop Real-Time Integration Methods Mech. Syst. Simul.*, 1990, pp. 193–207.
[41] O. Bauchau and A. Laulusa, "Review of contemporary approaches for constraint enforcement in multibody systems," *J. Comput. Nonlinear Dyn.*, vol. 3, 2008, Art. no. 011005.
[42] M. Benedikt, G. Stettinger, and M. Horn, "Sliding mode control for constraint stabilization in multi-body system dynamic analysis," in *Proc. IEEE Conf. Control Appl.*, 2014, pp. 1557–1562.
[43] S.-T. Lin and J.-N. Huang, "Stabilization of Baumgarte's method using the Runge-Kutta approach," *J. Mech. Des.*, vol. 124, pp. 633–641, 2002.
[44] H. Sparschuh and P. Hagedorn, "On the Gauss principle in the numerical integration of mechanical systems," in *Proc. NATO Adv. Res. Workshop Real-Time Integration Methods Mech. Syst. Simul.*, 1990, pp. 294–300.
[45] U. M. Ascher, C. Hongshen, and S. Reich, "Stabilization of DAEs and invariant manifolds," *Numerische Mathematik*, vol. 67, pp. 131–149, 1994.
[46] D. S. Bernstein, *Scalar, Vector, and Matrix Mathematics: Theory, Facts, and Formulas-Revised and Expanded Edition*. Princeton, NJ, USA: Princeton University Press, 2018.
[47] M. Benzi, G. H. Golub, and J. Liesen, "Numerical solution of saddle point problems," *Acta Numer.*, vol. 14, no. 1, pp. 1–137, 2005.
[48] G. H. Golub and C. F. Van Loan, *Matrix Computations*, 4th ed. Baltimore, MD, USA: Johns Hopkins University Press, 2013.
[49] E. Buckingham, "On physically similar systems; Illustrations of the use of dimensional equations," *Phys. Rev.*, vol. 4, no. 4, 1914, Art. no. 345.
[50] D. Arthur and S. Vassilvitskii, "k-means: The advantages of careful seeding," in *Proc. 18th Annu. ACM-SIAM Symp. Discrete Algorithms, Soc. Ind. Appl. Math.*, 2007, pp. 1027–1035.

Boyang Zhang (Student Member, IEEE) received the B.Eng. degree from Tianjin University, Tianjin, China, and the M.Eng. degree from Memorial University of Newfoundland, St. John's, NL, Canada, both in ocean and naval architectural engineering in 2013 and 2017, respectively. He is currently working toward the Ph.D. degree at the Department of Civil and Environmental Engineering, Duke University, Durham, NC, USA.

His research interests include dynamics, control, and optimization, with applications to multiagent robotics.

Henri P. Gavin received the B.S.E. degree from Princeton University, Princeton, NJ, USA, and the M.Eng. and Ph.D. degrees from University of Michigan, Ann Arbor, MI, USA, in 1986, 1988, and 1994, respectively, all in civil engineering.

He has been with Duke University, Durham, NC, USA, since 1995, where he is currently the Yoh Family Bass Professor with the Department of Civil and Environmental Engineering and Department of Mechanical Engineering and Materials Science. His research interests include nonlinear dynamics, optimal control, system identification, and stochastic optimization, with applications to earthquake engineering and multiagent systems.

Dr. Gavin was the recipient of the National Science Foundation Early CAREER Award, ASCE Walter L. Huber Civil Engineering Research Prize, Alumni Distinguished Undergraduate Teaching Award, and Earl I Brown II Outstanding Civil Engineering Faculty Award in 1996, 2005, 2008, and 2013, respectively. In 2010, he was the recipient of President's Award from New Zealand Society for Earthquake Engineering. He is a Bass Fellow and a Fellow of Japan Society for the Promotion of Sciences (2002).